Journal of Ginseng Research 48 (2024) 454–463

Contents lists available at ScienceDirect

Journal of Ginseng Research

journal homepage: www.sciencedirect.com/journal/journal-of-ginseng-research

Research Article

Structural analysis, anti-inflammatory activity of the main water-soluble acidic polysaccharides (AGBP-A3) from *Panax quinquefolius* L berry

Zhihao Zhang [a,b,1], Huijiao Yan [a,1], Hidayat Hussain [c], Xiangfeng Chen [a], Jeong Hill Park [d], Sung Won Kwon [d], Lei Xie [a], Bowen Zheng [b], Xiaohui Xu [f], Daijie Wang [a,b,*], Jinao Duan [e,**]

[a] *Shandong Analysis and Test Center, Qilu University of Technology (Shandong Academy of Sciences), Jinan, China*
[b] *Biological Engineering Technology Innovation Center of Shandong Province, Heze Branch of Qilu University of Technology (Shandong Academy of Sciences), Heze, China*
[c] *Department of Bioorganic Chemistry, Leibniz Institute of Plant Biochemistry, Halle (Saale), Germany*
[d] *College of Pharmacy and Research Institute of Pharmaceutical Sciences, Seoul National University, Seoul, Republic of Korea*
[e] *Jiangsu Collaborative Innovation Center of Chinese Medicinal Resources Industrialization, and Jiangsu Key Laboratory for High Technology Research of TCM Formulae, College of Pharmacy, Nanjing University of Chinese Medicine, Nanjing, China*
[f] *Department of Genetics and Cell Biology, Basic Medical College, Qingdao University, Qingdao, Shandong, China*

ARTICLE INFO

Keywords:
Panax quinquefolius L berry
Polysaccharides
Structural elucidation
Anti-inflammation
Molecular docking

ABSTRACT

Background: *Panax quinquefolius* L, widely recognized for its valuable contributions to medicine, has aroused considerable attention globally. Different from the extensive research has been dedicated to the root of *P. quinquefolius*, its berry has received relatively scant focus. Given its promising medicinal properties, this study was focused on the structural characterizations and anti-inflammatory potential of acidic polysaccharides from the *P. quinquefolius* berry.

Materials and methods: *P. quinquefolius* berry was extracted with hot water, precipitated by alcohol, separated by DEAE-52-cellulose column to give a series of fractions. One of these fractions was further purified via Sephadex G-200 column to give three fractions. Then, the main fraction named as AGBP-A3 was characterized by methylation analysis, NMR spectroscopy, etc. Its anti-inflammatory activity was assessed by RAW 264.7 cell model, zebrafish model and molecular docking.

Results: The main chain comprised of α-L-Rhap, α-D-GalAp and β-D-Galp, while the branch consisted mainly of α-L-Araf, β-D-Glcp, α-D-GalAp, β-D-Galp. The RAW264.7 cell assay results showed that the inhibition rates against IL-6 and IL-1β secretion at the concentration of 625 ng/mL were 24.83 %, 11.84 %, while the inhibition rate against IL-10 secretion was 70.17 % at the concentration of 312 ng/mL. In the zebrafish assay, the migrating neutrophils were significantly reduced in number, and their migration to inflammatory tissues was inhibited. Molecular docking predictions correlated well with the results of the anti-inflammatory assay.

Conclusion: The present study demonstrated the structure of acidic polysaccharides of *P. quinquefolius* berry and their effect on inflammation, providing a reference for screening anti-inflammatory drugs.

1. Introduction

Panax quinquefolius L, a perennial araliaceous herb, has been one of the most widely used medicinal herbs in the world [1]. *P. quinquefolius* was successfully introduced in China and is now grown widely in many areas, such as Shandong, Liaoning and Heilongjiang Province of China [2]. Studies have shown that *P. quinquefolius* had positive effects due to its wide range of biological activities and unique pharmacological effects [3,4]. Similar to *P. quinquefolius*, *P. quinquefolius* berry is a multiuse fruit containing bioactive compounds such as ginsenosides, polysaccharides, flavonoids, volatile oils, sterols et al. [5,6]. However, relatively few studies of practical purification methods for *P.*

* Corresponding author. Shandong Analysis and Test Center, Qilu University of Technology (Shandong Academy of Sciences), Jinan, China.
** Corresponding author. Jiangsu Collaborative Innovation Center of Chinese Medicinal Resources Industrialization, and Jiangsu Key Laboratory for High Technology Research of TCM Formulae,College of Pharmacy, Nanjing University of Chinese Medicine, Nanjing, China.
E-mail addresses: wangdaijie@qlu.edu.cn (D. Wang), dja@njutcm.edu.cn (J. Duan).
[1] These authors contributed equally to this work.

https://doi.org/10.1016/j.jgr.2024.05.001
Received 13 January 2024; Received in revised form 4 May 2024; Accepted 4 May 2024
Available online 8 May 2024

quinquefolius berry unitary active ingredient and their structural characteristics and biological activities have been fully researched.

Literature reports have focused on the study of crude extracts of *P. quinquefolius* berries. For example, berry extracts have shown anticancer action *in vitro* and *in vivo* tests [7]. In addition, *P. quinquefolius* berry extracts also provided protection against cardiac oxidaive stress [8] and enhanced the chemopreventive action of 5-FU's on the human colorectal carcinoma cells [9]. Another study found that *P. quinquefolius* berry extracts protected hepatocytes against APAP-induced hepatotoxicity by suppressing oxidative stress and inflammatory responses through TNF-α-mediated caspase-3/-8/-9 pathways [10]. The above research emphasized the biological activities of *P. quinquefolius* berry extract, but did not the specific components of the extract. As noted above, *P. quinquefolius* berry contained polysaccharides. Polysaccharides are a kind of natural active substance existing in plants, animals and microorganisms, etc. They are composed of many monosaccharide residues connected by α or β glycoside bonds, usually more than 10 monosaccharides polymerized into polysaccharide. Its relative molecular weight varies from tens of thousands to millions [11]. Thus, polysaccharides have a complex structure and variable monosaccharide composition. There are also vital factors in the broad-spectrum bioactivities of polysaccharides. Extensive studies have shown that polysaccharides possessed biological activity, such as immunomodulatory [12], antioxidant [13], anti-inflammatory [14], anti-cancer [15], etc. In recent years, there are an increased numbers of reports on polysaccharides. As natural products, polysaccharides are good scaffolds for the development of potent drugs. Moreover, natural products form the basis for new chemical entities with different molecular structures and have been shown to be highly relevant to drug find [16,17].

In the present work, the specific structure of a homogeneous acidic polysaccharide from *P. quinquefolius* berry, were identified and analyzed using molecular weight determination, methylation assay, monosaccharide composition assessment, FT-IR spectroscopy and 1D/2D NMR. Moreover, the anti-inflammatory activity of *P. quinquefolius* berry acidic polysaccharides were also evaluated using the zebrafish experiments and *in vitro* inflammatory factors secretion level test. Molecular docking was accomplished to further verify the AGBP-A3's anti-inflammatory effects.

2. Material and method

2.1. Material and chemical

P. quinquefolius berry were purchased from Shandong Baicaotang Chinese Herbal Pieces Co., Ltd. Monosaccharide standards, including arabinose, fructose, fucose, galactose, galacturonic acid, glucose, glucosamine hydrochloride, guluronic acid, glucuronic acid, galactose hydrochloride, mannose, N-acetyl-D-glucosamine, ribose, rhamnose and xylose, used for ion chromatography were procured from Yuanye Bio Technology (Shanghai, China). BoRui Saccharide Biotech (Yangzhou, China) was the supplier of Sephadex G-200, diethylaminoethyl (DEAE)-Sepharose Fast Flow resin and the carbohydrate methylation kit used in this study. *Tg* (*lyz*: *DsRed2*) strain zebrafish and RAW 264.7 cells were provided by the Institute of Drug Research, Shandong Academy of Medical Sciences'. All other reagents were analytical grade.

2.2. Extraction of polysaccharide

The crude polysaccharide was obtained by slightly modifying earlier research methods [18]. The smashed *P. quinquefolius* berry was extracted with distilled water (1:30, *v/w*) twice for 1.5 h at 80 °C. The combined solution was concentrated at 65 °C to get rid of parts water. The concentrated sample was centrifuged at 6000 r/min for 10 min to produce a clear solution. The supernatant was then diluted with 95 % ethanol (1:4, *v/v*) and the mixture was left to stay at 4 °C for overnight. The precipitates were then collected by centrifugation to get the crude polysaccharides from *P. quinquefolius* berry. The crude polysaccharides were then diluted with distilled water, deproteinated by using the sevage reagent (chloroform/*n*-butanol, 4:1, *v/v*) [19], dialyzed for 48 h in a 3500 Da dialysis bag, and lyophilized to yield the deproteinated crude polysaccharides for further analysis.

2.3. Isolation and purification of polysaccharide

Crude polysaccharides were dissolved, centrifuged and then loaded on a pre-equilibrated DEAE-52-cellulose column at a flow rate of 1.5 mL/min, followed by an elution step with distilled water, 0.2 M, 0.5 M, 1.0 M NaCl solution. A rotary vacuum evaporator was utilized to concentrate the fraction at 65 °C, followed by 48 h dialysis in a 1000 Da dialysis bag and subsequent freeze-drying. Four elution fractions were obtained. The fractions eluted with 0.2 M NaCl were further purified on a Sephadex G-200 column. The NaCl solution (0.2 M) was eluent at a flow rate of 0.2 mL/min. The resulting solution was dialyzed for 48 h in a 1000 Da dialysis bag followed by freeze-drying. The polysaccharide fractions (AGBP-A3) obtained were used for further analysis [20].

2.4. Structural analysis of AGBP-A3

2.4.1. Molecular weight determination

The molecular weight of AGBP-A3 was determined by the high-performance gel-permeation chromatography [21]. Samples and standards were accurately weighed, a 5 mg/mL solution was prepared, centrifuged, filtered, and transferred to a 2.0 mL feed vial. The Shimadzu LC-10 A system was utilized, which was equipped with a RI-502 differential detector and 8 mm × 300 mm BRT105-104-102 column. The standard curve was plotted using the commercial dextran standards with different molecular weights (5.0, 11.6, 23.8, 48.6, 80.9, 148.0, 273.0, 409.8, 670.0 KDa). The molecular mass of AGBP-A3 was estimated based on the standard curve. NaCl solution (0.05 M) was used as the flow phase, with a flow rate of 0.6 mL/min; the injection volume and column temperature settings were 20 μL and 40 °C separately.

2.4.2. Monosaccharide composition determination

The monosaccharide composition was assessed as per a prior procedure [22]. First, AGBP-A3 (5 mg) was hydrolyzed for 3 h at 120 °C with 2 M trifluoroacetic acid (TFA 2 mL) in a sealed ampoule bottle. The resulting hydrolysate was dried under nitrogen flow to remove residual TFA and then dissolved in 5 mL of distilled water. The above sample solution was used 50 μL and added 950 μL of deionized water. An ICS5000 ion chromatograph was utilized to examine the hydrolyzed product AGBP-A3, coupled to a 3 × 150 mm DionexCarbopac^{TM}PA20 column and an electrochemical probe. Uronic acids reduction was performed using uronic acid reduction apparatus supplied by BoRui Saccharide Biotech (Yangzhou, China). The mobile phases were A (H_2O), B (15 mM NaOH), and C (15 mM NaOH & 100 mM NaOAc) with flow rates of 0.3 mL/min; the column temperature and injection volume were set separately at 30 °C and 5 μL.

2.4.3. FT-IR analysis

AGBP-A3 (2 mg) was mixed with 200 mg of dried KBr and pressed into sheets. The KBr powder was used as a blank control. FT-IR 650 (Tianjin Gangdong Sci. &Tech. Co., Ltd.) spectrometer (range: 4000-400 cm^{-1}) was utilized to perform the FT-IR analysis [22].

2.4.4. Methylation analysis

Dried AGBP-A3 (2–3 mg) was dissolved in anhydrous DMSO (2 mL). After adding reagent A (aqueous alkali solution), the samples were quickly sealed and subjected to ultrasound treatment, then incubated for 30 min at room temperature. The samples were then mixed with reagent B (methyl iodide) for methylation purpose, and stirred for 5 h under N_2 protection at 30 °C. This reaction was discontinued by adding 2 mL of ultrapure water. The resulting solution was dialyzed for 48 h at 4 °C

against ultrapure water. The methylated polysaccharides were then extracted thrice extraction with dichloromethane, dried over sodium sulfate and evaporated to dryness. After 2 h of hydrolysis with 3 mol/L TFA (2 mL) at 120 °C, ultrapure water (1 mL) and $NaBH_4$ (100 mg) were utilized to evaporate and reduce the methylated samples for 12 h. Subsequently, the reduced polysaccharide was subjected to neutralization with acetic acid, evaporation, drying at 100 °C and acetylation with acetic anhydride. Finally, GC-MS system was used to examine the acetylated products [18].

GC-MS experiment was used an RXI-5 SIL MS column with a size of 30 m × 0.25 mm × 0.25 μm. The temperature protocol was an initial adjustment to 120 °C, increased at 3 °C/min to 250 °C, and held for 5 min. High purity helium (99.999 %) was used as the carrier gas, with constant flow rate of 1.0 mL/min. The temperatures of the injection port, ion source and transfer line were all set at 250 °C.

2.4.5. NMR analysis

AGBP-A3 (50 mg) was dissolved in 99.9 % D_2O (0.5 mL) and freeze-dried. Dissolution and freeze-drying were repeated three times, resulting in a full exchange of active hydrogen. Then ^1H and ^{13}C NMR spectra were recorded on a Bruker-600 MHz NMR spectrometer at room temperature.

2.5. Anti-inflammatory activity based on RAW264.7 cell model

2.5.1. Cell culture

Murine macrophage-like RAW264.7 cells, provided by the Pharmaceutical Institute (Shandong Province, China), were cultured at 37 °C in RAW264.7 cells specific medium under a humidified 5 % CO_2 atmosphere. The cells were incubated overnight and used in subsequent experiments.

2.5.2. Assessment of cell viability

Cells viability was assessed by the methyl thiazolyl tetrazolium (MTT) reduction colorimetric assay [23]. Firstly, 1×10^5 cells were seeded per well of a 96-well microplate. AGBP-A3 was then added at different concentrations (78, 156, 312, 625, 1250, 2500, and 5000 ng/mL) at 37 °C. After 24 h of incubation, 1.0 mg/mL MTT was added to the cells in each well and allowed to stand for 4 h. The supernatants were then discarded, and the formazan crystals were solubilized with dimethyl sulfoxide (DMSO; 100 μL). A Tristar2 S LB 942 microplate reader was utilized to determine the absorbance at 570 nm.

2.5.3. Determination of inflammatory factors levels

After culturing, 1×10^5 RAW264.7 cells were seeded into each well of 96-well microplates and grown to confluence. The drug was administered according to the LPS (1 μg/mL) model, the control, and the drug + LPS groups. The administration concentrations of AGBP-A3 were set at 156, 312, 625 and 2500 μg/mL. After 24 h treatment, the cells were removed from the incubator and the cell culture supernatant was collected for assay according to the kit operating instructions. IL-6, IL-1β, and IL-10 inflammatory factors were included.

2.6. Anti-inflammatory activity based on zebrafish model

Zebrafish were placed in a mating tank in a 2:2 male to female ratio. Male and female fish were isolated. They were also kept at a fixed temperature of 28 ± 0.5 °C under a 14 h light/10 h dark photocycle. After 24 h, male and female zebrafish mate and reproduce, obtaining fertilized eggs. After washing, these fertilized eggs were transferred into tanks filled with methylene blue-involving embryo medium. Finally, these embryos were cultured at 28 °C for later experiments [24]. The zebrafish experiment compiled with the National Research Council's Guide for the Care and Use of Laboratory Animals and was approved by the Animal Ethics Committee of the Biology Institute of Shandong Academy of Sciences (protocol No: SWS20230615).

Zebrafish embryos were incubated up to 3 dpf. Screening of normally developed zebrafish in six-well plates with a total volume of 5 mL per well, male to female ratio 1:1, 30 strips/well. Then ten zebrafish/group were randomly selected for the experiment. In addition to the copper sulfate model, ibuprofen-positive drug and blank control groups, various concentrations (10, 20, 50 and 100 μg/mL) of experimental sample groups were also set. After 6 h of pre-protection, all groups except the blank control were added with 3.2 g/L copper sulfate mother solution (5 μL). The inflammatory response was observed and photographed. Fluorescent microscope was used to observe the neutrophil distribution in zebrafish. The number of neutrophils migrating to and above the lateral line neuromast was also statistically analyzed.

2.7. Molecular docking

Using Molecular Operating Environment (MOE, 2008), the compounds were subjected to molecular docking analysis against the COX-2 target. The amino acid sequences of COX-2 exhibited inter-species conservation, with a similarity range of 85–90 %. The structure of human COX-2 was anticipated to very similar to that of the mouse enzyme, as the two structures are conserved strictly at the active site and share an 87 % identity [25]. Protein Data Bank (http://www.rcsb.org) was the source of data concerning the COX-2's crystal structures with PDB ID 1CX2. After the removal of water molecules and other ligands, hydrogen atoms were introduced and protein crystal structures were minimized and optimized. Protonation states were assumed to be the most common at pH 7. The active sites were displayed in the set finder by MOE. Prior to the completion of relative docking, the target polysaccharides and ibuprofen were prepared by converting the Chem3D and ChemDraw files into the SDF ones. The alpha triangle was selected as the placement index. London dG was chosen to score the results. Ligand interaction was used to check out the connections between COX-2 and polysaccharides. H bonds had pronounced effect on the biomolecular functionality and structure, and the analysis of actual ligand-receptor interactions was based on the H bonding.

2.8. Data analysis

Data were reported as means ± standard deviations. Differences were assessed for significance using one-way analysis of variance (ANOVA) using Graphpad Prism 8.0Differences were considered significant at $p < 0.05$ and high significant at $p < 0.01$.

3. Results and discussion

3.1. Isolation and purification

The whole process is schematically shown in Fig. 1A. Crude polysaccharides were extracted from *P. quinquefolius* berry, using hot water followed by ethanol precipitation and deproteinization. The crude polysaccharide had a yield of 6.32 % (31.6 g from 500 g dried *P. quinquefolius* berry). Four polysaccharide fractions of were acquired after separation on a glass column of DEAE-Sepharose Fast Flow. Ultrapure water was utilized to elute the neutral fraction, while 0.2, 0.5 and 1.0 M NaCl were used separately to elute the rest 3 acidic fractions (Fig. 1B). The yields of the four components (neutral fraction, 0.2, 0.5 and 1.0 M NaCl fractions) were 9.3 %, 10 %, 4.1 % and 0.9 %, respectively. This fraction was further purified on a Sephadex G-200 column (Fig. 1C). Three peaks were observed. The symmetrical parts of the three peaks were collected and named AGBP-A1, AGBP-A2, and AGBP-A3. The respective yields were 3.2 %, 8.2 %, and 17.0 %. AGBP-A3 was further investigated as the main polysaccharide fraction.

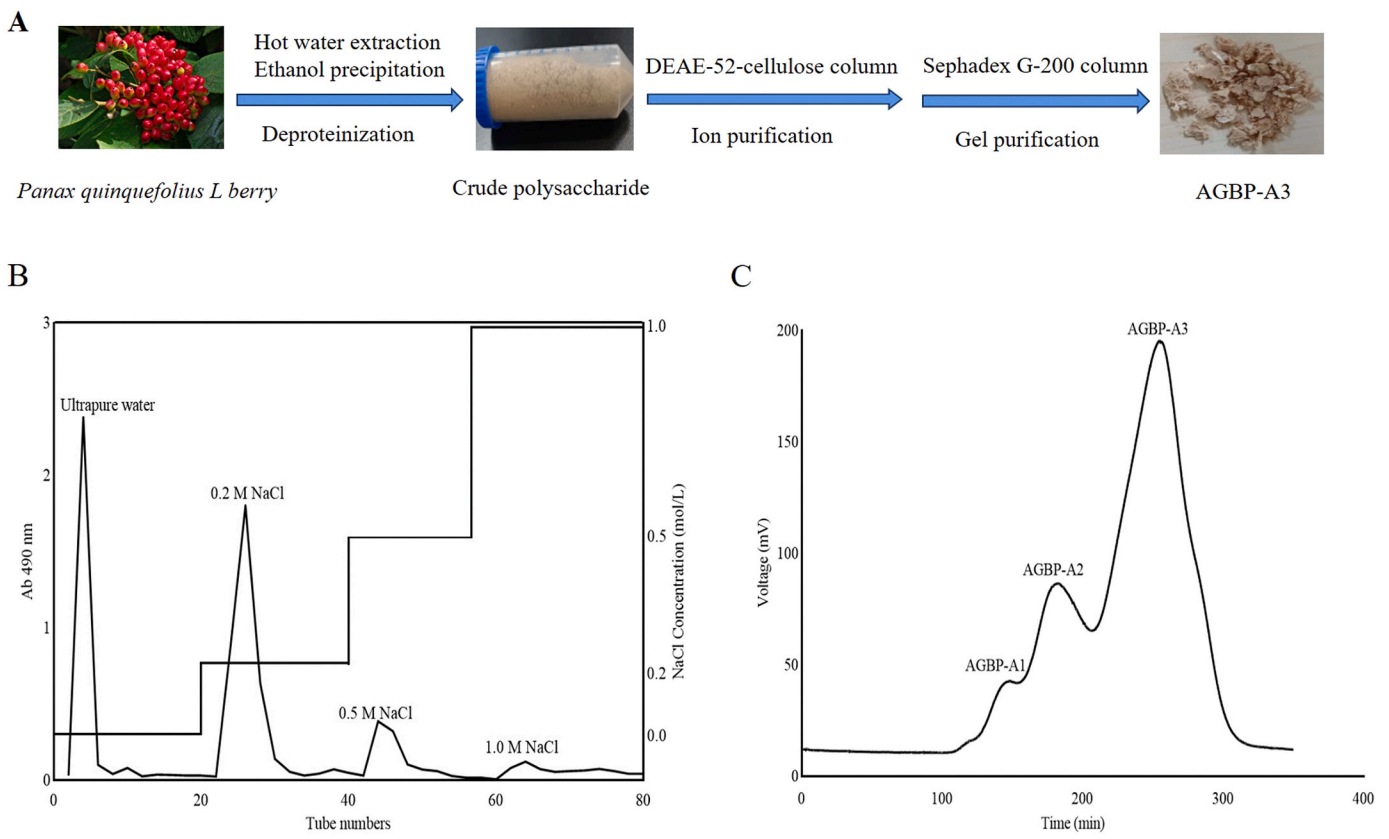

Fig. 1. Extraction, isolation and purification of AGBP-A3. (A) whole process (extraction, separation, purification); (B) Elution curve of AGBP-A3 on DEAE-Sepharose Fast Flow column; (C) Elution curve of AGBP-A3 on Sephadex G-200 column.

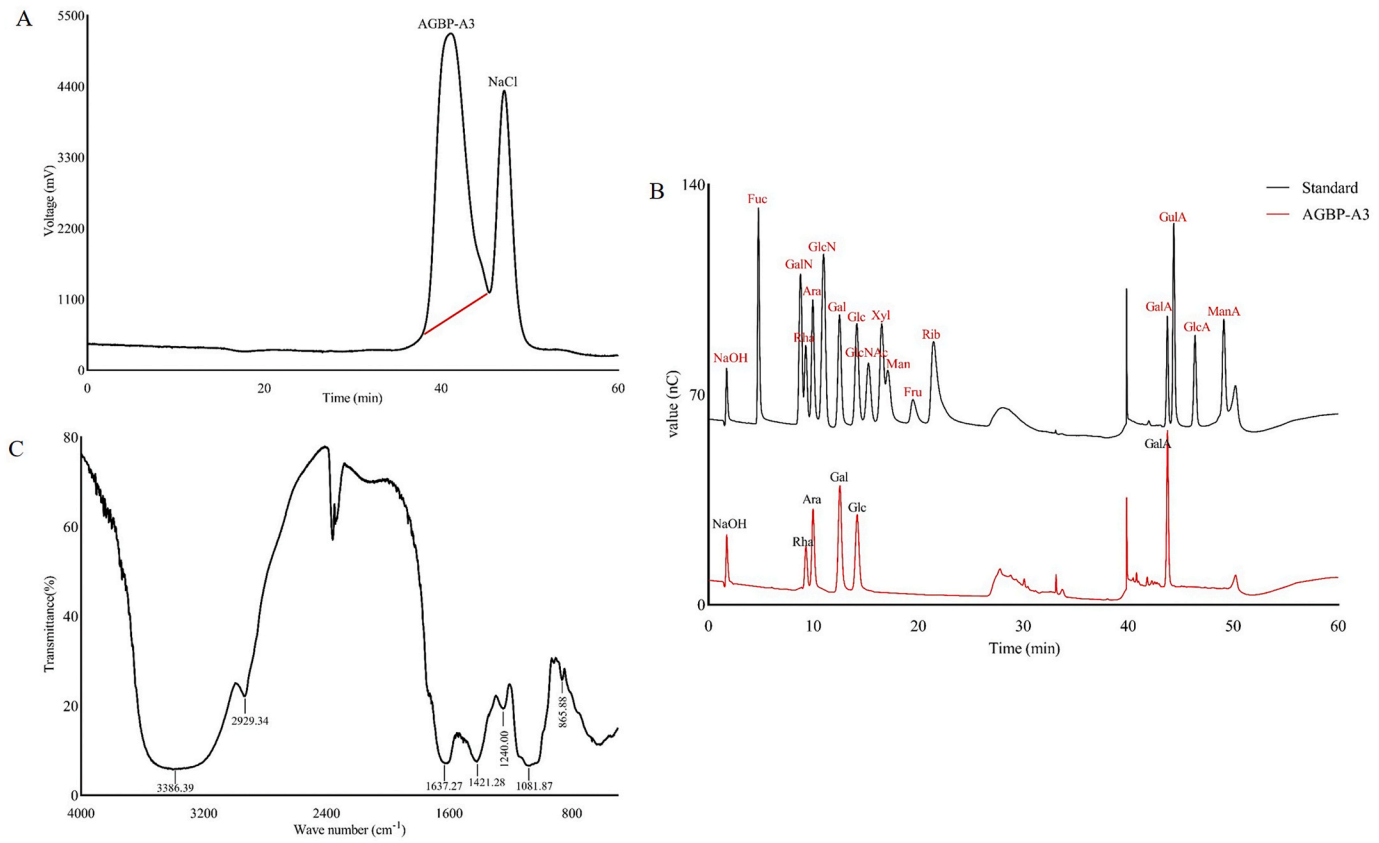

Fig. 2. Structure analysis of AGBP-A3. (A) HPGPC elution curve of AGBP-A; (B) Monosaccharide composition analysis of AGBP-A3; (C) FT-TR spectrum of AGBP-A3.

3.2. Structure elucidation of AGBP-A3

3.2.1. Molecular weight analysis

The relative molecular mass was evaluated via the HPGPC system. As displayed in Fig. 2A, a sharp symmetrical peak appeared in the elution profiles of AGBP-A3's, suggesting its homogeneity. In addition, the peak in 47.0 min was signal of the flow phase. The standard curve was calculated as follows: lgMw = 12.602–0.2001t, lgMn = 11.858–0.1856t, where Mw and Mn are the weight and number-average molecular masses respectively, and t is the retention time, with correlation coefficients of 0.9947 and 0.9941. The Mw and Mn of AGBP-A3 were calculated as 24060 Da, 17100Da, and a retention time of 41.083 min. The dispersion index (Mw/Mn) was 1.407.

3.2.2. Analysis of monosaccharide composition

Ion chromatography was employed to identify the monosaccharide composition of AGBP-A3 by comparing retention times with standard monosaccharides. As shown in Fig. 2B, the results indicated that AGBP-A3 consisted of Rha, Ara, Gal, Glc, GalA, in molar ratios of 0.137: 0.136: 0.225: 0.175: 0.327. The molar ratio of Rha/GalA indicated the contribution of RG-I to polysaccharide population. The (Ara + Gal)/Rha reflected the average length of RG-I side chains [26,27]. Rha/GalA was 0.42 and (Ara + Gal)/Rha was 2.64, suggesting that the AGBP-A3 has abundant RG-I structural domains with long Ara and Gal side chains. After uronic acids reduction, Rha, Ara, Gal, Glc, GalA were detected respectively. The molar ratios were 0.118: 0.123: 0.551: 0.163: 0.045, the amount of GalA was significantly reduced.

3.2.3. FT-IR analysis

As shown in Fig. 2C, the FT-IR spectra of AGBP-A3 showed typical bands characteristic of polysaccharides. The absorption peak at 3386 cm^{-1} was assigned to the O–H stretching vibration of the constituent glucose residues, which was the characteristic peak of sugars [19]. The absorption peak at 2929 cm^{-1} was attributed to the stretching vibration of C–H in the sugar ring, while the peak at 1637 cm^{-1} corresponded to the asymmetric C═O stretching vibration [28]. This indicates that AGBP-A3 is an acidic polysaccharide. The strong absorption peaks appearing at 1421 cm^{-1} and 1081 cm^{-1} were probably attributed to the stretching vibration of C–O [29]. The peak 1240 cm^{-1} represented the S═O stretching vibration of sulfate groups [30]. In addition, the absorption peak at 865 cm^{-1} was attributed to a feature of the pyranose hypomethyl deformation vibration [31]. Taken together, it might be deduced that AGBP-A3 was an acidic polysaccharide and the exact structure needs to be further combined with methylation and NMR.

3.2.4. Methylation analysis

Peak identification for the partially methylated alditol acetates in the GC-MS data was made according to their retention times and by comparative analysis with the Complex Carbohydrate Research Center database. The ratio of each sugar was determined from the peak area in the GC-MS data. Table S1 shows the molar ratios, mass fragmentation profiles, as well as glycosyl linkage patterns. There were thirteen types of glycosidic bonds in AGBP-A3, namely Araf-(1→, →2)-Rhap-(1→, →5)-Araf-(1→, Glcp-(1→, Galp-(1→, →3,5)-Araf-(1→, →2,4)-Rhap-(1→, →3)-Galp-(1→, →4)-Galp-(1→, →4)-Glcp-(1→, →6)-Galp-(1→, →3,4)-Galp-(1→, →3,6)-Galp-(1→ at molar ratios of 0.0354: 0.0843: 0.0607: 0.0333: 0.1199: 0.0757: 0.0765: 0.1297: 0.2335: 0.0320: 0.0156: 0.0792: 0.0242.

3.2.5. NMR analysis

Further structural elucidation of AGBP-A3 was carried out by the NMR spectrum. In the ^{1}H NMR spectrum (Fig. 3A), the primary range of ^{1}H spectrum signals were δ 3.50 to δ 5.70 ppm. For anomeric ^{1}H protons, their chemical shift positions were within δ 4.80 to δ 5.80 ppm, suggesting that the sugar residues existence α configuration. The chemical shift positions were within δ 4.30-δ 4.80 ppm, suggesting that the sugar residues exist in β configuration. The ^{1}H NMR spectrum pinpointed the main signals of anomeric protons at δ 5.70, 5.22, 5.17, 5.16, 5.04, 5.01, 4.97, 4.96, 4.83, 4.55, 4.55, 4.52, 4.46, 4.45, 4.44 ppm, corresponding to H-1 of F, M, A, L, D, C, E, B, G, J, K, O, H, N, I. The main range of signals in the ^{13}C NMR spectrum (Fig. 3B) was from δ 60 to δ 120 ppm. Signals were seen for 15 anomeric carbons at δ 110.62, 108.90, 108.88, 108.77, 108.18, 105.39, 104.90, 104.48, 104.30, 104.20, 103.84, 101.34, 100.38, 99.88, 99.80 ppm which corresponded to C-1 of A, D, C, B, F, J, I, N, K, O, H, G, E, M, L.

A further structural assessment of AGBP-A3 was accomplished by 2D NMR including NEOSY, HMBC, ^{1}H–^{13}C HSQC and ^{1}H–^{1}H COSY. The spectra were shown in Figures C–F. For the analysis of the ^{1}H and ^{13}C signals of the glycosyl residues', the HSQC spectra (Fig. 3C), COSY spectra (Fig. 3D), monosaccharide composition, methylation data, and NMR data reported in the literature were utilized. For instance, over the residue →4)-α-D-GalAp-(1→ (E), an anomeric carbon signal of δ 100.3 ppm can be observed in the HSQC spectrum, corresponding to an anomeric proton signal of δ 4.97 ppm. In the ^{1}H–^{1}H COSY spectra, the cross peaks at $\delta_{H1/H2}$4.97/3.67, $\delta_{H2/H3}$3.67/3.93, $\delta_{H3/H4}$3.93/4.32, $\delta_{H4/H5}$4.32/4.68, indicate that the signals at δ 4.97, 3.67, 3.93, 4.32 and 4.68 ppm correspond respectively to H-1, H-2, H-3, H-4 and H-5. In addition, the corresponding C1–C5 carbon signals were 100.3, 69.4, 70.0, 79.1, and 72.6 ppm [32]. Similarly, further information can be deduced about additional residues: residue α-L-Araf-(1→(A, B), →5)-α-L-Araf-(1→(C), →3, 5)-α-L-Araf-(1→(D) [13,33]; residue α-D-GalAp-(1→(F), →3,4)-α-D-GalAp-(1→(G) [34,35]; residue β-D-Galp-(1→(N), →6)-β-D-Galp-(1→(I), →3)-β-D-Galp-(1→(J), →3, 6)-β-D-Galp-(1→(K) [36,37]; residue →2,4)-α-L-Rha-(1→(L), →2)-α-L-Rha-(1→(M) [38]; residue β-D-Glcp-(1→ (O), →4)-β-D-Glcp-(1→(H) [39]. The attribution of all glycosidic bond signals is shown in Table S2.

Polysaccharide substitution sites, backbone, and glycosyl residues were analyzed by NOESY (Fig. 3E) and HMBC spectra (Fig. 3F). The master chain was analyzed as follows. NOESY ($\delta_{H/H}$) and HMBC ($\delta_{H/C}$) spectra exhibited correlated peaks M(H-1)/L(H-2) at $\delta_{H/H}$ 5.22/4.06, L (H-1)/E(C-4) at $\delta_{H/C}$ 5.16/79.1, E(H-1)/E(H-4) at $\delta_{H/H}$ 4.97/4.32, E(H-1)/G(H-4) at $\delta_{H/H}$ 4.97/4.48, G(H-1)/G(H-4) at $\delta_{H/H}$ 4.83/4.48, G (H-1)/K(C-6) at $\delta_{H/C}$ 4.83/70.6, K(H-1)/I(H-6) at $\delta_{H/H}$ 4.55/3.89. As a result, several structural inter-residual sequences were conjectured to be the occurrence of →2)-α-L-Rhap-(1 → 2,4)-α-L-Rhap-(1→[4)-α-D-GalAp-(1]$_2$ → 3,4)-α-D-GalAp-(1 → 3,4)-α-D-GalAp-(1 → 3,6)-β-D-Galp-(1 → 6)-β-D-Galp-(1 → . In the light of the above correlations, α-L-Rhap, α-D-GalAp and β-D-Galp was likely connected and formed the polysaccharide backbone. The branched chain was analyzed as follows. HMBC spectrum correlations between A(H-1)/C(C-5) at $\delta_{H/C}$ 5.17/68.2, C(H-1)/D(C-5) at $\delta_{H/C}$ 5.01/67.80, B(H-1)/D(C-3) at $\delta_{H/C}$ 4.96/83.6 and D(H-1)/L(C-4) at $\delta_{H/C}$ 5.04/76.8 implied the occurrence of a non-linear side chain as T-α-Araf-(1 → 5)-α-Araf-(1 → 5)[T-α-Araf-(1 → 3]-α-Araf-(1 → . This branch is linked to C-4 of L. The correlations between O(H-1)/H(H-4) at $\delta_{H/H}$ 4.52/3.64, H(H-1)/H(H-4) at $\delta_{H/H}$ 4.46/3.64, N (H-1)/J(H-3) at $\delta_{H/H}$ 4.45/3.77 indicate the existence of the linkage β-D-Glcp-(1→[4)- β-D-Glcp-(1]$_2$, β-D-Galp-(1 → 3)-β-D-Galp-(1. In addition, additional HMBC ($\delta_{H/C}$) and NOESY ($\delta_{H/H}$) correlated peaks were assigned to H(H-1)/G(C-3) at $\delta_{H/C}$ 4.46/82.55, F(H-1)/G (H-3) at $\delta_{H/H}$ 5.70/4.09, J(H-1)/K(H-3) at $\delta_{H/H}$ 4.55/3.81, which indicated that the H residue in the side chain was directly boned to the C-3 position of the residue G's, and that F, J were separately bonded to the C-3 of the G, K residues C.

Accordingly, the structure information of AGBP-A3, the structure was postulated as illustrated in Fig. 3G, taking into account the comprehensive outcomes of monosaccharide composition, NMR and methylation assays. Depending on the results of the molecular weight determination, the n value is 8 or 9.

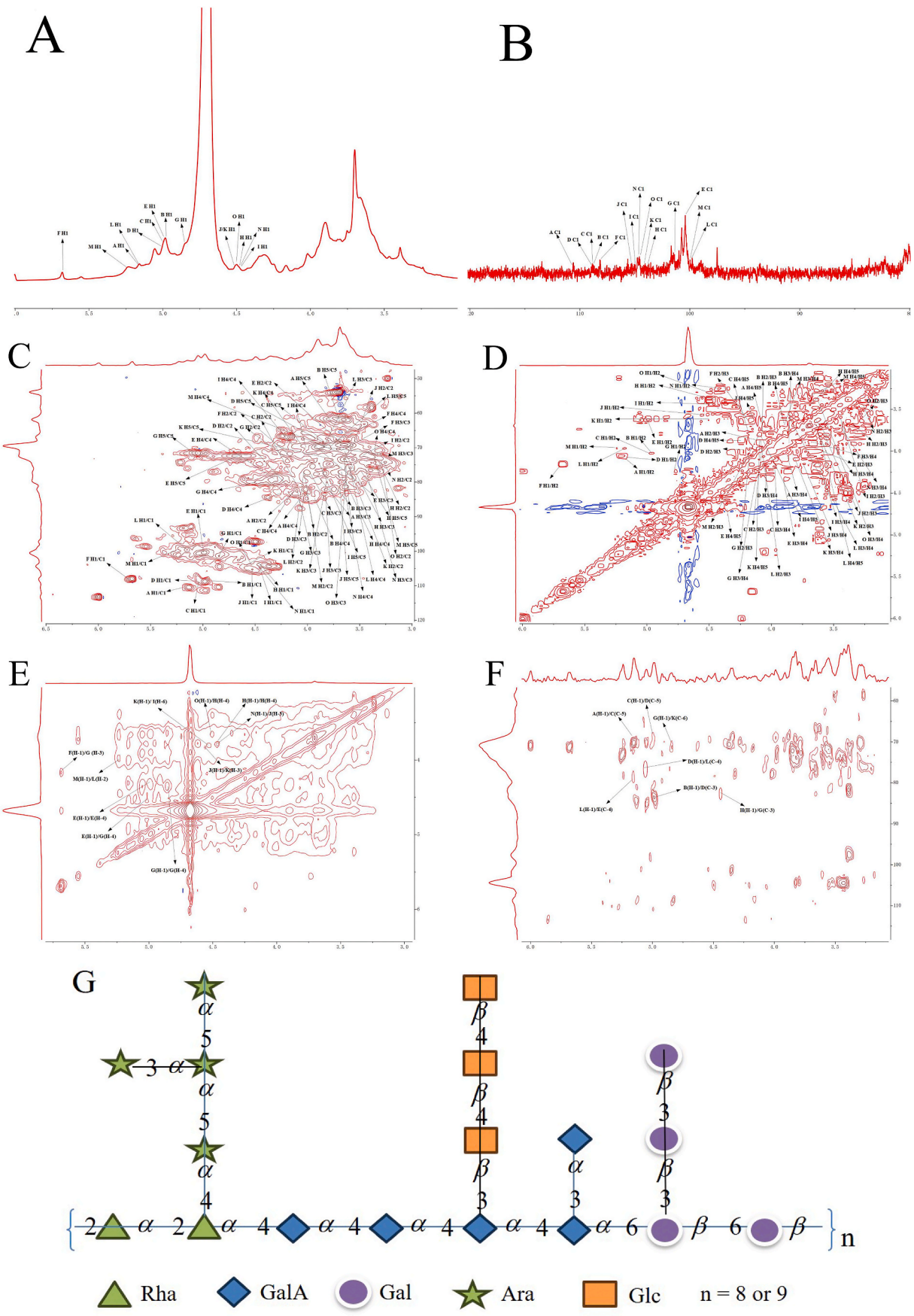

Fig. 3. NMR spectra of AGBP-A3. (A)^{1}H spectrum; (B) ^{13}C spectrum; (C) HSQC; (D) ^{1}H–^{1}H COSY; (E) NOESY; (F) HMBC; (G) Putative structure of AGBP-A3.

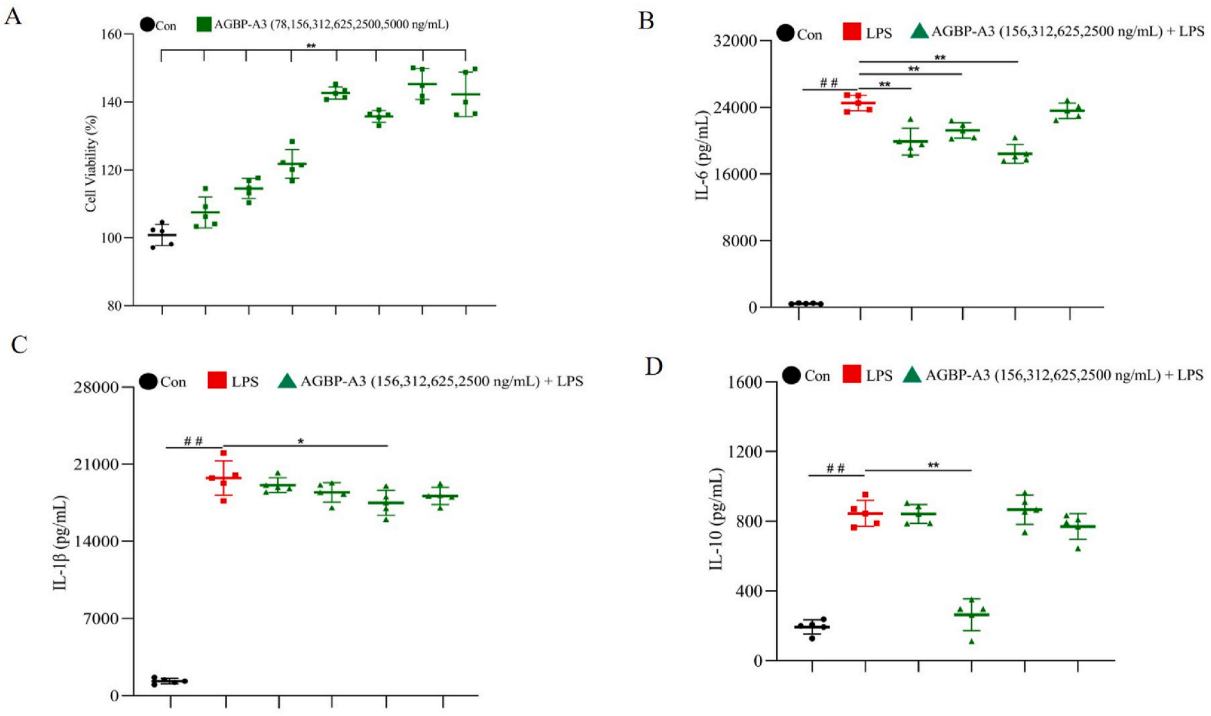

Fig. 4. The effect of AGBP-A3 on the secretion of IL-6, IL-1β, IL-10. (A) cells viability; (B) IL-6; (C) IL-1β; (D) IL-10. Data were presented as mean ± standard deviation (n = 5). LPS model group vs con (untreated group), ##$P < 0.01$. Data vs LPS model group, *$P < 0.05$, **$P < 0.01$.

3.3. *In vitro and in vivo anti-inflammatory activity of AGBP-A3*

3.3.1. *Cell viability effects of AGBP-A3*

In order to verify the toxicity of AGBP-A3 against RAW264.7 cells, the MTT assay was conducted to evaluate the cell viability. The results showed a lack of cytotoxicity against RAW264.7 cells at doses of 78, 156, 312, 625, 1250, 2500, and 5000 ng/mL of AGBP-A3 (Fig. 4A). Survival rates were greater than 95 % in the control and all treatments, suggesting that the polysaccharide samples did not cause cytotoxicity at tested doses. Hence, the range of these concentration was selected for future anti-inflammatory experiments.

3.3.2. *Secretion levels of IL-10, IL-6, and IL-1β*

Numerous diseases and pathologies, including neurodegenerative disorders, diarrhea, sepsis and respiratory infections, are associated with the lipopolysaccharide (LPS)-induced inflammation [40]. As a physiological response, inflammation involved a series of complex interactions between immunocytes and soluble factors. Research showed that excessive release of pro-inflammatory cytokines (IL-10, IL-6 and IL-1β) and mediators (NO) was closely linked to the pathogenesis of inflammation [41]. Therefore, in our research, 1 μg/mL LPS was used to produce the cell inflammation model, and IL-6, IL-1β and IL-10 secretion levels were measured after the addition of different concentrations of AGBP-A3.

As sown in Fig. 4B, the IL-6 levels secreted by the RAW264.7 cells were significantly increased by LPS in contrast to the control ($p < 0.01$). This suggested that LPS successfully induced inflammation in RAW264.7 cells. The IL-6 secretion was reduced by AGBP-A3 treatment in contrast to the model group. There were statistically significant differences at AGBP-A3 concentrations of 156, 312, and 625 ng/mL compared to the model group ($p < 0.01$). The inhibition was 24.83 % at 625 ng/mL. As indicated in Fig. 4C–D, the pro-inflammatory cytokine discharges were significantly higher in the model group than in the control group ($p < 0.01$). When the LPS-stimulated RAW264.7 cells were treated with AGBP-A3, the IL-1β and IL-10 discharges were reduced to some extent. In Fig. 4C, there was statistical difference at 625 ng/mL when compared to the model group ($p < 0.05$). The inhibition rate was 11.34 %. As presented in Fig. 4D–a significant difference from the model group ($p < 0.01$) was observed for AGBP-A3 at 312 ng/mL. The inhibition rate was 70.17 %. The above results indicate that AGBP-A3 inhibits LPS-induced inflammation in RAW 264.7 cells at a range of concentrations.

3.3.3. *Zebrafish model*

Despite being a micronutrient in a particular concentration range, copper can be harmful to many types of cells if its intracellular concentration is unbalanced. In zebrafish, excessive environmental copper disturbed the Cu balance, triggers inflammatory reactions mediated by oxidative stress [42]. The progression of inflammation and oxidative stress was accompanied by the activation of neutrophils and macrophages and the overproduction of reactive oxygen species (ROS). As a type of innate immunocytes, neutrophils were the first cells in tissues to be recruited to sites of inflammation [43]. In the present study, the zebrafish inflammation model was established using $CuSO_4$ to test the effects of AGBP-A3's effects on the neutrophils numbers y and migration of upon Cu^{2+} stimulation of the zebrafish.

As shown in Fig. 5A, in the absence of $CuSO_4$ stimulation, localization of almost whole neutrophils was observed in the posterior abdominal and tail hematopoietic tissues of the blank control. There was migration of the neutrophils to the site of inflammation when stimulated with $CuSO_4$, with cluster formation at the lateral line neuromast. Neutrophils migration was attenuated and the number of fluorescent spots was reduced after AGBP-A3 treatment. According to the quantitative outcomes, the copper sulfate model group exhibited significantly different amount of migrated neutrophils from the ibuprofen-positive drug group. After treatment with different concentrations of AGBP-A3, a decrease in the number of migrated neutrophil counts was observed. Compared to the model group, the 50, 100 μg/mL was significantly different ($p < 0.01$). There was no statistical difference at 10, 20 μg/mL (Fig. 5B). The inhibition rates were 23.77 % and 27.81 % for AGBP-A3 concentrations of 50 and 100 μg/mL, respectively. The results indicate that AGBP-A3 at certain concentrations can reduce the number of

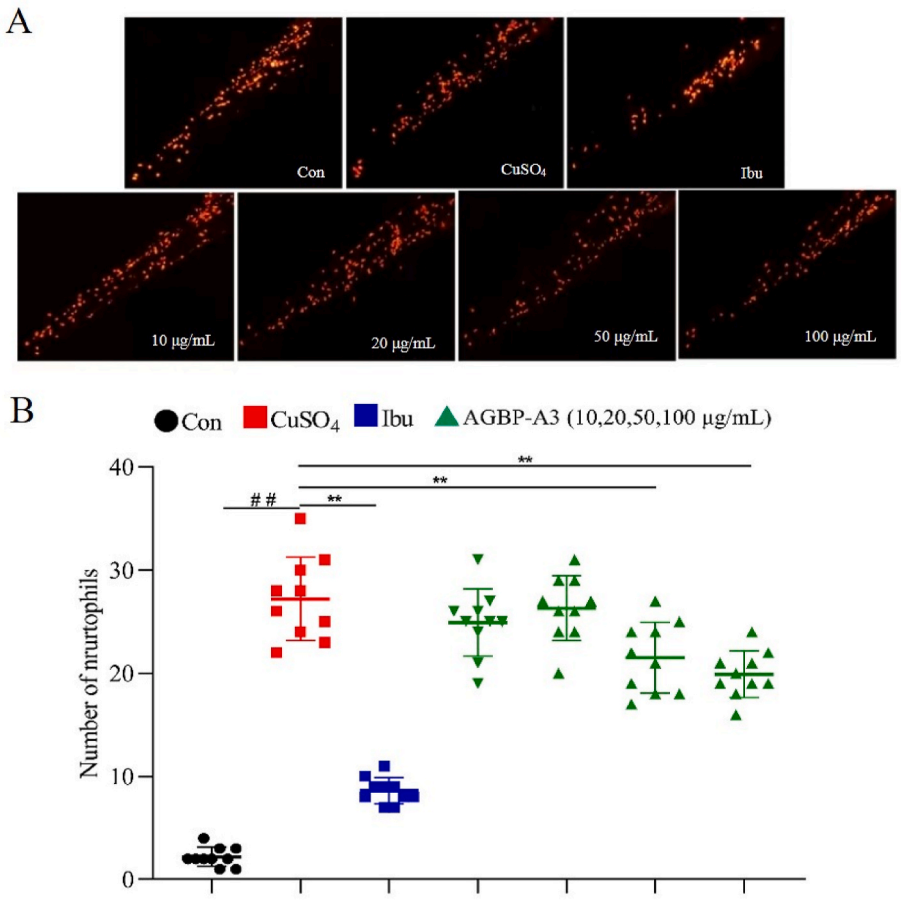

Fig. 5. The effect of AGBP-A3 on $CuSO_4$-induced zebrafish inflammation model. (A) The observation of neutrophil migration; (B)The quantitative results of neutrophil migration. Data were presented as mean ± standard deviation (n = 10). $CuSO_4$ model group vs Con (untreated group), $\#\#P < 0.01$. Data vs $CuSO_4$ model group, $^{*}P < 0.05$, $^{**}P < 0.01$.

migrated neutrophil and thereby suppress the $CuSO_4$-induced inflammatory response to some extent.

Summary to the above date, AGBP-A3 showed significant anti-inflammatory activity with the monosaccharide composition of arabinose and galactose et al., and the branch chain of α-L-Araf, β-D-Glcp, α-D-GalAp, and β-D-Galp. Rod-in et al. [44,45] found that the main polysaccharides in *P. quinquefolius* berry was rhamnose (14.1 %), arabinose (26.8 %), glucose (26.7 %), and galactose (24.5 %), which was similar to the present research of AGBP-A3. Pharmacological studies showed that the polysaccharides composed of galactose and arabinose had the significant anti-inflammatory activity. Ye et al. [46] founded that high contents fucose and galactose in sulfated fucoidan of *Saccharina japonica* possessed the high anti-inflammatory activity. Gong et al. [47] reported that high contents of arabinose and galactose significantly improved the anti-inflammatory activity of the *Lycium barbarum* polysaccharide fraction by increasing NO levels, phagocytosis, and acid phosphatase in RAW 264.7 cells. Sanjeewa et al. [48] demonstrated that sulfated polysaccharides with high contents of fucose and galactose isolated from *Sargassum horneri* could markedly reduce the production of inflammatory cytokines and prostaglandin E2 in LPS-stimulated RAW 264.7 cells and protecte zebrafish embryos from LPS-induced NO production and death. Therefore, the high content of arabinose and galactose in AGBP-A3 may contribute the anti-inflammatory activity in acidic polysaccharide from *P. quinquefolius* berry.

3.4. Molecular docking analysis

According to the docking results, AGBP-A3 displayed diverse binding interactions and a satisfactory binding score. In contrast to the polysaccharide, the 1CX2 binding energies of ibuprofen were lower (Table S3), indicating that it was more affinitive towards the selected protein. The results of the docking predictions were correlated well with *in vitro* experimental finding. The lowest binding energy of AGBP-A3 at the active site was −11.33 kcal/mol. The ligand formed strong hydrogen bonds with Thr118 (2.87 Å), Gln370 (1.22, 1.88 and 2.46 Å) and weak hydrogen bonds with Thr118 (3.34 and 3.82 Å), Gln370 (3.48 Å) (Fig. 6). The strong hydrogen bonds suggest considerable binding capacity, which could influence and interact with COX-2. The weak hydrogen bonds may modify docking stabilities and structural packing models.

Prostaglandin is a latent inflammatory mediator [49]. In inflammatory cells, endotoxins, cytokines and mitogens can induce COX-2, which is responsible for the elevated prostaglandins production during inflammation. In fact, molecular docking studies have further supported the inhibitory action of polysaccharides' and facilitated better understanding of various interactions between the enzyme active sites and ligands. One potential to alleviate the inflammatory response is to decrease the level of COX-2's activity [50].

4. Conclusion

In this study, the *P. quinquefolius* berry were extracted with hot water, precipitated with alcohol and separated on a DEAE-52-cellulose column to obtain a series of fractions. One of the fractions was further purified by Sephadex G-200 column to obtain three polysaccharide fractions. The purified major polysaccharide fraction was then further

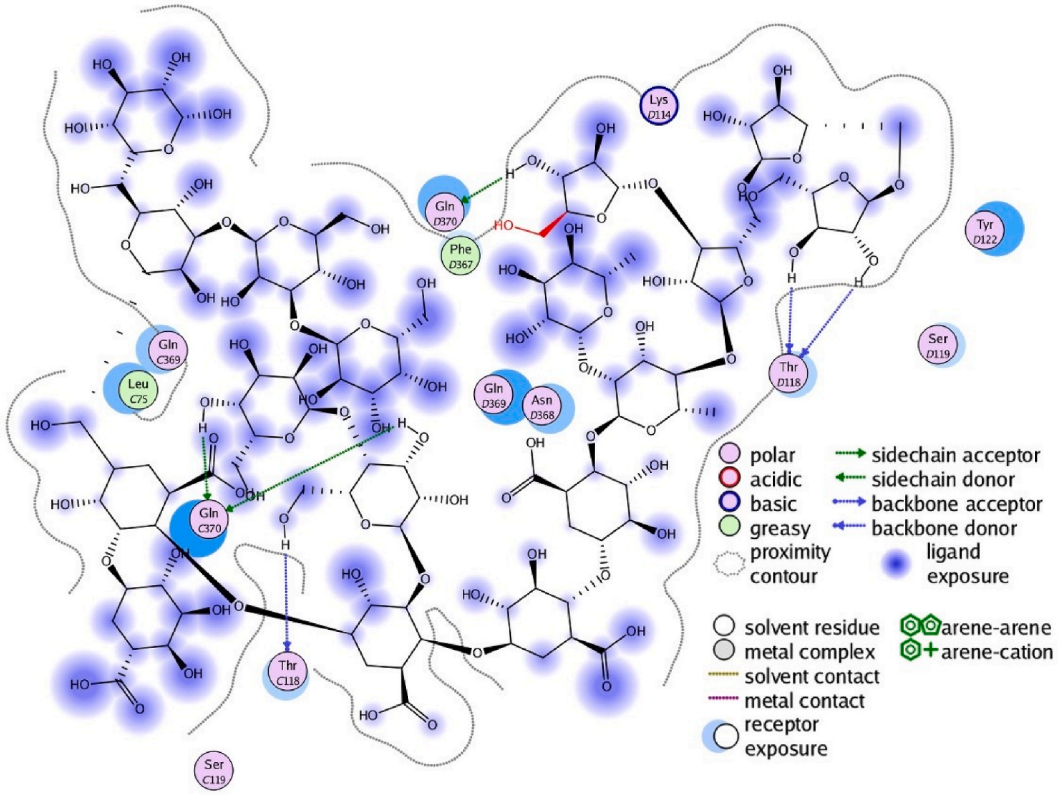

Fig. 6. Ligand interaction of AGBP-A3 with 1CX2.

analyzed. Structural analyses showed that AGBP-A3 primarily consisted mainly of α-L-Rhap, α-D-GalAp and β-D-Galp while the branch consisted mainly of α-L-Araf, β-D-Glcp, α-D-GalAp, and β-D-Galp. The anti-inflammatory activity of *P. quinquefolius* berry acidic polysaccharide was also evaluated using the zebrafish experiments and the inflammatory factors secretion level test. The results of molecular docking assays were highly correlated with *in vivo* and *in vitro* activity assays. All results showed excellent anti-inflammatory activity, which may due to its monosaccharide composition, complex structure, etc. This requires further research structure-activity relationship.

Associated contents

Supplementary Material: Table S1 Methylation analyses of AGBP-A3. Table S2 ^{1}H and ^{13}C NMR chemical shifts of AGBP-A3. Table S3 Docking scores of ibuprofen and AGBP-A3 to Cyclooxygenase −2 (PDB ID: 1CX2).

Ethical approval

There were no any studies on human participants contained in this article. All applicable guidelines followed for the use and care of animals were institutional, national, and international.

Acknowledgement

We gratefully acknowledge the Science, Education and Industry Integration Innovation Pilot Project from Qilu University of Technology (Shandong Academy of Sciences) (2022JBZ02-06), Key R&D Program of Shandong Province (2023TZXD068, 2023TZXD083), the Science and Technology smes Innovation Ability Improvement Project of Shandong Province (2022TSGC2439), the Key R&D and transformation plan of Qinghai Province (2023-SF-112), and the assistance of Yangzhou BoRui Saccharide Biotech Co. Ltd. (www.polyscilife.com) in experiments design and data analysis.

Appendix A. Supplementary data

Supplementary data to this article can be found online at https://doi.org/10.1016/j.jgr.2024.05.001.

References

[1] Zhang J, Fan S, Qin J, Dai J, Zhao F, Gao L, Lian X, Shang W, Xu X, Hu X. Changes in the microbiome in the soil of an American ginseng continuous plantation. Front Plant Sci 2020;11:572199.
[2] Ma Xiu-li HC-y, Shi -xiang LU, Yun-xiu SUN, Ju-zheng LIU, Shu-ying LIU. Isolation and characterization of a bioactive polysaccharide from Panax quinquef olium L. Chem Res Chin Univ 1998;14(2):143–6.
[3] Assinewe VA, Arnason JT, Aubry A, Mullin J, Lemaire I. Extractable polysaccharides of Panax quinquefolius L. (North American ginseng) root stimulate TNFa production by alveolar macrophages. Phytomedicine 2002;9(5):398–404.
[4] Lemmon HR, Sham J, Chau LA, Madrenas J. High molecular weight polysaccharides are key immunomodulators in North American ginseng extracts: characterization of the ginseng genetic signature in primary human immune cells. J Ethnopharmacol 2012;142(1):1–13.
[5] Xie JT, Wu JA, Mehendale S, Aung HH, Yuan CS. Anti-hyperglycemic effect of the polysaccharides fraction from American ginseng berry extract in *ob/ob* mice. Phytomedicine 2004;11(2–3):182–7.
[6] Wang C, Song W. Steamed American ginseng berry: ginsenoside analyses and anticancer activities. J Agric Food Chem 2006;54:9936–42.
[7] Xie J, Wang C, Zhang B. In vitro and in vivo anticancer effects of American ginseng berry: exploring representative compounds. Biol Pharm Bull 2009;32(9):1552–8.
[8] Mehendale SR, Wang CZ, Shao ZH, Li CQ, Xie JT, Aung HH, Yuan CS. Chronic pretreatment with American ginseng berry and its polyphenolic constituents attenuate oxidant stress in cardiomyocytes. Eur J Pharmacol 2006;553(1–3):209–14.
[9] Wang C, Sun S. American ginseng berry enhances chemopreventive effect of 5-FU on human colorectal cancer cells. Oncol Rep 2009;22(4):943–52.
[10] Xu XY, Wang Z, Ren S, Leng J, Hu JN, Liu Z, Chen C, Li W. Improved protective effects of American ginseng berry against acetaminophen-induced liver toxicity through TNF-alpha-mediated caspase-3/-8/-9 signaling pathways. Phytomedicine 2018;51(7):128–38.
[11] Li J, Huang G. Extraction, purification, separation, structure, derivatization and activities of polysaccharide from Chinese date. Process Biochem 2021;110(9):231–42.

[12] Fan H, Sun M, Li J, Zhang S, Tu G, Liu K, Xia Q, Jiang Y, Liu B. Structure characterization and immunomodulatory activity of a polysaccharide from Saposhnikoviae Radix. Int J Biol Macromol 2023;233:123502.
[13] Zhang H, Zou P, Zhao H, Qiu J, Regenstein JM, Yang X. Isolation, purification, structure and antioxidant activity of polysaccharide from pinecones of Pinus koraiensis. Carbohydr Polym 2021;251:117078.
[14] Bai Y, Zhou Y, Zhang R, Chen Y, Wang F, Zhang M. Gut microbial fermentation promotes the intestinal anti-inflammatory activity of Chinese yam polysaccharides. Food Chem 2023;402:134003.
[15] Qiu WL, Lo HC, Lu MK, Lin TY. Significance of culture period on the physiochemistry and anti-cancer potentials of polysaccharides from mycelia of Ganoderma lucidum. Int J Biol Macromol 2023;242(4):125181.
[16] Mallavadhani UV, Chandrashekhar M, Nayak VL, Ramakrishna S. Synthesis and anticancer activity of novel fused pyrimidine hybrids of myrrhanone C, a bicyclic triterpene of Commiphora mukul gum resin. Mol Divers 2015;19(4):745–57.
[17] Chandrashekhar M, Nayak VL, Ramakrishna S, Mallavadhani UV. Novel triazole hybrids of myrrhanone C, a natural polypodane triterpene: synthesis, cytotoxic activity and cell based studies. Eur J Med Chem 2016;114:293–307.
[18] Li G, Chen P, Zhao Y, Zeng Q, Ou S, Zhang Y, Wang P, Chen N, Ou J. Isolation, structural characterization and anti-oxidant activity of a novel polysaccharide from garlic bolt. Carbohydr Polym 2021;267:118194.
[19] Chen W, Zhu X, Ma J, Zhang M, Wu H. Structural elucidation of a novel pectin-polysaccharide from the petal of saussurea laniceps and the mechanism of its anti-HBV activity. Carbohydr Polym 2019;223:115077.
[20] Zhang M, Wang G, Lai F, Wu H. Structural characterization and immunomodulatory activity of a novel polysaccharide from lepidium meyenii. J Agric Food Chem 2016;64(9):1921–31.
[21] Zhou Y, Wang S, Feng W, Zhang Z, Li H. Structural characterization and immunomodulatory activities of two polysaccharides from Rehmanniae Radix Praeparata. Int J Biol Macromol 2021;186:385–95.
[22] Song H, Han L, Zhang Z, Li Y, Yang L, Zhu D, Wang S, He Y, Liu H. Structural properties and bioactivities of pectic polysaccharides isolated from soybean hulls. LWT - Food Sci Technol (Lebensmittel-Wissenschaft -Technol) 2022;170:114079.
[23] Brahmi F, Hadj-Ahmed S, Zarrouk A, Bezine M, Nury T, Madani K, Chibane M, Vejux A, Andreoletti P, Boulekbache-Makhlouf L, Lizard G. Evidence of biological activity of Mentha species extracts on apoptotic and autophagic targets on murine RAW264.7 and human U937 monocytic cells. Pharmaceut Biol 2017;55(1):286–93.
[24] Li JJ, Zhang Y, Han LW, Tian QP, He QX, Wang XM, Sun C, Han J, Liu KC. Tenacissoside H exerts an anti-inflammatory effect by regulating the nf-kappab and p38 pathways in zebrafish. Fish Shellfish Immunol 2018;83:205–12.
[25] Filipponi E, Cecchetti V, Fravolini A. Chemometric rationalization of the structural and physicochemical basis for selective cyclooxygenase-2 inhibition: toward more specific ligands. J Comput Aided Mol Des 2000;14:277–91.
[26] Li Q, Li J, Li H, Xu R, Yuan Y, Cao J. Physicochemical properties and functional bioactivities of different bonding state polysaccharides extracted from tomato fruit. Carbohydr Polym 2019;219:181–90.
[27] Wang W, Ma X, Jiang P, Hu L, Zhi Z, Chen J, Ding T, Ye X, Liu D. Characterization of pectin from grapefruit peel: a comparison of ultrasound-assisted and conventional heating extractions. Food Hydrocolloids 2016;61:730–9.
[28] Yang B, Luo Y, Sang Y, Kan J. Isolation, purification, structural characterization, and hypoglycemic activity assessment of polysaccharides from Hovenia dulcis (Guai Zao). Int J Biol Macromol 2022;208:1106–15.
[29] Wang S, Yang Y, Xiao D, Zheng X, Ai B, Zheng L, Sheng Z. Polysaccharides from banana (Musa spp.) blossoms: isolation, identification and anti-glycation effects. Int J Biol Macromol 2023;236:123957.
[30] Bhadja P, Tan C, Ouyang J, Yu K. Repair effect of seaweed polysaccharides with different contents of sulfate group and molecular weights on damaged HK-2 cells. Polymers 2016;8(5):188.
[31] Wei Q, Zhang YH. Ultrasound-assisted polysaccharide extraction from Cercis chinensis and properites, antioxidant activity of polysaccharide. Ultrason Sonochem 2023;96:106422.
[32] Kim M, Kim SR, Park J, Mun SH, Kwak M, Ko HJ, Baek SH. Structure and antiviral activity of a pectic polysaccharide from the root of Sanguisorba officinalis against enterovirus 71 in vitro/vivo. Carbohydr Polym 2022;281:119057.
[33] Ye J, Zhang C, Lyu X, Hua X, Zhao W, Zhang W, Yang R. Structure and physicochemical properties of arabinan-rich acidic polysaccharide from the by-product of peanut oil processing. Food Hydrocolloids 2021;117:106743.
[34] Makarova EN, Shakhmatov EG. Characterization of pectin-xylan-glucan-arabinogalactan proteins complex from Siberian fir Abies sibirica Ledeb. Carbohydr Polym 2021;260:117825.
[35] Shen Y, Liang J, Guo YL, Li Y, Kuang HX, Xia YG. Ultrafiltration isolation, structures and anti-tumor potentials of two arabinose- and galactose-rich pectins from leaves of Aralia elata. Carbohydr Polym 2021;255:117326.
[36] Huang W, Zhao M, Wang X, Tian Y, Wang C, Sun J, Wang Z, Gong G, Huang L. Revisiting the structure of arabinogalactan from Lycium barbarum and the impact of its side chain on anti-ageing activity. Carbohydr Polym 2022;286:119282.
[37] Rakhmanberdyeva RK, Shashkov AS, Bobakulov KM, Azizov DZ, Malikova MK, Ogay DK. The structure and prebiotic activity of arabinogalactan from Ferula Kuhistanica. Carbohydr Res 2021;505:108342.
[38] Liu Q, Fang J, Wang P, Du Z, Li Y, Wang S, Ding K. Characterization of a pectin from LonicerajaponicaThunb and its inhibition effect on $AF062_{42}$ aggregation and promotion of neuritogenesis. Int J Biol Macromol 2018;107:112–20.
[39] Liu W, Li W, Sui Y, Li XQ, Liu C, Jing H, Zhang H, Cao W. Structure characterization and anti-leukemia activity of a novel polysaccharide from Angelica sinensis (Oliv.) Diels. Int J Biol Macromol 2019;121:161–72.
[40] Zheng ZH, Tu JL, Li XH, Hua Q, Liu WZ, Liu Y, Pan BX, Hu P, Zhang WH. Neuroinflammation induces anxiety- and depressive-like behavior by modulating neuronal plasticity in the basolateral amygdala. Brain Behav Immun 2021;91:505–18.
[41] Zhang H, Guo Q, Liang Z, Wang M, Wang B, Sun-Waterhouse D, Waterhouse GIN, Wang J, Ma C, Kang W. Anti-inflammatory and antioxidant effects of Chaetoglobosin V(b) in LPS-induced RAW264.7 cells: achieved via the MAPK and NF-kappaB signaling pathways. Food Chem Toxicol 2021;147:111915.
[42] Pereira TC, Campos MM, Bogo MR. Copper toxicology, oxidative stress and inflammation using zebrafish as experimental model. J Appl Toxicol 2016;36(7):876–85.
[43] Zhang Q, Ding A, Yue Q, Li W, Zu Y, Zhang Q. Dynamic interaction of neutrophils and RFP-labelled Vibrio parahaemolyticus in zebrafish (Danio rerio). Aquaculture and Fisheries 2017;2(6):269–77.
[44] Li H, Rod-in W, Surayot U, You S, Park WJ. Inhibitory effects of polysaccharides from Korean ginseng berries on LPS-induced RAW264.7 macrophages. PLoS One 2023;18(11).
[45] Talapphet N, Rod-in W, Monmai C, Jang Ay, You S, Park WJ. Immune enhancement effects of Korean ginseng berry polysaccharides on RAW264.7 macrophages through MAPK and NF-κB signalling pathways. Food Agric Immunol 2021;32(1):298–309.
[46] Ye J, Chen D, Ye Z, Huang Y, Zhang N, Lui EMK, Xue C, Xiao M. Fucoidan isolated from Saccharina japonica inhibits LPS-induced inflammation in macrophages via blocking NF-κB, MAPK and JAK-STAT pathways. Mar Drugs 2020;18(6).
[47] Gong G, Dang T, Deng Y, Han J, Zou Z, Jing S, Zhang Y, Liu Q, Huang L, Wang Z. Physicochemical properties and biological activities of polysaccharides from Lycium barbarum prepared by fractional precipitation. Int J Biol Macromol 2018;109:611–8.
[48] Sanjeewa KKA, Fernando IPS, Kim S-Y, Kim H-S, Ahn G, Jee Y, Jeon Y-J. In vitro and in vivo anti-inflammatory activities of high molecular weight sulfated polysaccharide; containing fucose separated from Sargassum horneri: short communication. Int J Biol Macromol 2018;107:803–7.
[49] Sadiq A, Mahnashi MH, Alyami BA, Alqahtani YS, Alqarni AO, Rashid U. Tailoring the substitution pattern of Pyrrolidine-2,5-dione for discovery of new structural template for dual COX/LOX inhibition. Bioorg Chem 2021;112:104969.
[50] Lee YR, Moon GH, Shim D, Kim JC, Lee KJ, Chung KH, An JH. Neuroprotective effects of fermented tea in MPTP-induced Parkinson's disease mouse model via MAPK signaling-mediated regulation of inflammation and antioxidant activity. Food Res Int 2023;164:112133.